EurJIC European Journal of Inorganic Chemistry

ChemPubSoc Europe

FULL PAPER

DOI:10.1002/ejic.201403091

Al^{3+}-Ion-Triggered Conformational Isomerization of a Rhodamine B Derivative Evidenced by a Fluorescence Signal – A Crystallographic Proof

Buddhadeb Sen,[a] Siddhartha Pal,[a] Samya Banerjee,[b] Somenath Lohar,[a] and Pabitra Chattopadhyay*[a]

Keywords: Isomerization / Aluminum / Rhodamine derivatives / Structure elucidation / Fluorescence

A newly designed rhodamine B anisaldehyde hydrazone exhibits Al^{3+}-ion-induced *cis* (**L**) to *trans* (**L′**) conformational isomerization with respect to the xanthene moiety through a rotation about a N–N bond; the isomerization is indicated by a detectable naked-eye color change and a turn-on red fluorescence in 4-(2-hydroxyethyl)-1-piperazineethanesulfonic acid (HEPES) buffer (EtOH/Water 1:9 v/v; pH 7.4) at 25 °C. In support of this observation, detailed spectroscopic and physicochemical studies along with density function theory (DFT) calculations have been performed. This *cis*-to-*trans* conformational isomerization is due to Al^{3+} ion coordination, which induces this visual color change and the turn-on fluorescence response. To strengthen our knowledge of the conformational isomerization, detailed structural characterizations of the *cis* and *trans* isomers in the solid state were performed by single-crystal X-ray diffraction. To the best of our knowledge, this is the first structural report of both *cis* and *trans* conformational isomers for this family of compounds. Moreover, this noncytotoxic probe could be used to image the accumulation of Al^{3+} ions in HeLa and MCF-7 cell lines.

Introduction

Rhodamines are an advantageous class of photostable dyes as their long-wavelength absorption with a high absorption coefficient and emission with excellent quantum efficiency make them competent fluorescent biomarkers.[1–3] Conformational isomerization plays a vital role in many biological systems for the transmission of information through the binding of an ion or molecule to another binding site, as structural changes result in dissimilarities in physiological activities and pharmacological effects.[4,5] Conformational isomerization is also significantly important in the design of ion-controlled switching devices and the manufacture of fine chemicals.[6–9] There are some reports on thermally induced and photoinduced *cis–trans* conformational isomerization,[10,11] but metal-ion-induced *cis–trans* conformational isomerization is scarce.[12] Herein, we describe the first observation of Al^{3+}-ion-induced *cis–trans* conformational isomerization, which was observed in a new rhodamine B derivative through detailed structural elucidations.

In this manuscript, we report a rhodamine B hydrazone derivative (**L**), which exhibits Al^{3+}-ion-induced isomerization from the *cis* conformation (**L**) to the *trans* conformation (**L′**) with respect to the xanthene moiety; the change is evidenced by a noticeable naked-eye color change and a turn-on red fluorescence signal. The selective transformation of the weakly fluorescent *cis* conformational isomer (**L**) to its corresponding *trans* conformational isomer (**L′**) within a short time through the addition of Al^{3+} ions was confirmed by structural characterization of the *trans* isomer (**L′**), which was isolated from the **L′**–Al complex upon treatment with F^- ions. Owing to the coordination of Al^{3+} ions to **L**, a rotation about the N–N bond results in the *cis–trans* conformational isomerization from **L** to **L′**.

This Al^{3+}-ion-induced selective isomerization of **L** has been ascertained by UV/Vis, ^1H NMR, and ^{13}C NMR spectroscopy and ESI-MS, and the detailed structural analyses of the *cis* and *trans* conformational isomers were established by single-crystal X-ray diffraction studies support by theoretical calculations. This is an interesting type of Al^{3+}-ion-induced conformational isomerization that signals through turn-on red fluorescence.

Results and Discussion

The *cis* derivative with respect to the xanthene moiety of the rhodamine B hydrazone (**L**) was isolated from the reaction of rhodamine B hydrazide with *ortho*-anisaldehyde in

[a] Department of Chemistry, The University of Burdwan, Golapbag, Burdwan, 713104, India
E-mail: pabitracc@yahoo.com
[b] Department of Inorganic and Physical Chemistry, Indian Institute of Science, Bangalore, 560012, India

Supporting information for this article is available on the WWW under http://dx.doi.org/10.1002/ejic.201403091.

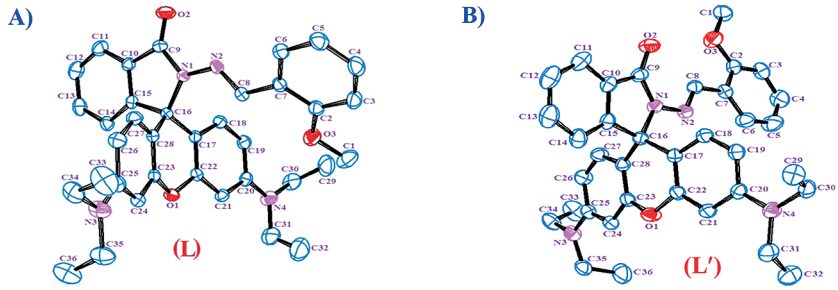

Figure 1. ORTEP views of (A) *cis* (**L**) and (B) *trans* (**L′**) conformers (30% probability) with atom numbering scheme (H atoms are excluded for clarity).

a 1:1 molar ratio in dry ethanol (Scheme 2). Crystals of **L** were collected after the slow evaporation of the reaction mixture over a few days and characterized by physicochemical and spectroscopic methods (Figures S1–S4, Supporting Information); these crystals were identical to the crystals obtained by the slow evaporation of a methanolic solution of **L**. The detailed structural analysis of **L**, which is in the *cis* conformation with respect to the xanthene moiety, was established by collecting the crystallographic data of a single crystal suitable for X-ray diffraction study (Figure 1, A, Table 1 and Supporting Information, Tables S1–S2). The crystal structure of **L** revealed the spirolactam configuration (spiro atom C-16) with the metal-chelating residue orthogonal to the oxotricyclic ring system of the rhodamine moiety, and this conformation makes the probes weakly fluorescent. Therefore, both rings are supposed to act as signal switchers, which show a turn-on response when bound to Al^{3+} ions.

Table 1. Crystal data and details of refinements for **L** and **L′**.

	L	**L′**
Empirical formula	$C_{36}H_{38}N_4O_3$	$C_{36}H_{38}N_4O_3$
Formula weight	574.70	574.70
Crystal system	triclinic	monoclinic
Space group	$P\bar{1}$	$P2_1/c$
a [Å]	9.9945(4)	13.0204(5)
b [Å]	11.6134(5)	11.8790(5)
c [Å]	15.4804(7)	20.0062(7)
α [°]	90.227(2)	90
β [°]	102.174(2)	95.061(2)
γ [°]	115.296(2)	90
Density [Mg/m^3]	1.209	1.238
Volume [Å^3]	1578.96(12)	3082.3(2)
Temperature [K]	296(2)	296(2)
Z	2	4
$F(000)$	612	1224
θ range [°]	2.478 to 28.293	2.668 to 28.359
Collected reflections	7793	7657
Independent reflections	5436	3789
Goodness-of-fit	1.049	1.030
$R1$ [$I > 2\sigma(I)$]	0.0497	0.0594
w$R1$ [$I > 2\sigma(I)$]	0.1244	0.1560

The UV/Vis spectrum of the *cis* isomer (**L**) in 4-(2-hydroxyethyl)-1-piperazineethanesulfonic acid (HEPES) buffer (1 mM, EtOH/water 1:9 v/v, pH 7.4) was recorded at 25 °C. The *cis* Isomer showed an absorption maximum at λ = 318–323 nm, which is attributed to the intramolecular π–π* charge-transfer (CT) transition. On stepwise addition of Al^{3+} ions (0–20 μM), a new absorption peak at $\lambda \approx 563$ nm gradually developed owing to the formation of an **L′**–Al complex through ring opening, and a visual color change from colorless to pink was observed (Figure 2). In the presence of excess biologically relevant alkali ions (Na^+, K^+), alkaline earth ions (Ca^{2+}, Mg^{2+}), transition metal ions (Cr^{3+}, Mn^{2+}, Fe^{3+}, Co^{2+}, Ni^{2+}, Cu^{2+}, Zn^{2+}, Cd^{2+}), and other heavy metal ions (Hg^{2+}, Pb^{2+}), no new bands were produced, as they were unable to induce the ring-opening step.

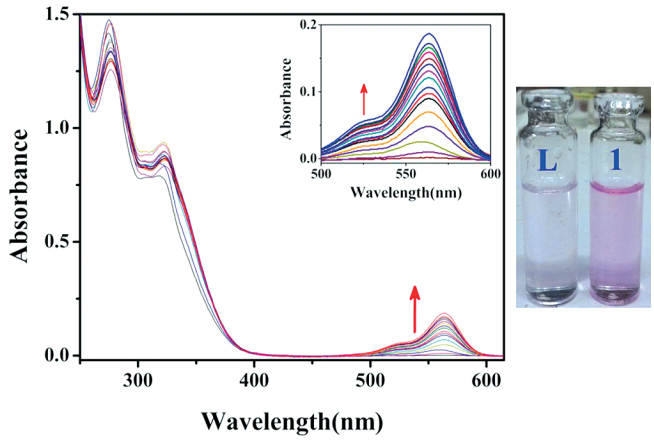

Figure 2. UV/Vis titration spectra of **L** (10 μM) in HEPES buffer (1 mM, EtOH/water 1:9 v/v, pH 7.4) at 25 °C upon the incremental addition of Al^{3+} ions (0–20 μM). Right: the naked-eye visual color change from **L** to **L′**–Al (**1**).

The *cis* conformational isomer (**L**) exhibited weak fluorescence at $\lambda \approx 580$ nm (λ_{ex} = 525 nm), which is independent of the pH of the medium over the range 6.0–10.0 (Figure S10). On the gradual addition of Al^{3+} ions to the solution of **L**, a fluorescence maximum at λ = 593 nm becomes visible with a redshift of 13 nm, and its intensity increased with Al^{3+} concentration to 2 equiv. (Figure 3). This strong fluorescence emission is due to the ring opening of the spirolactam system of rhodamine B (Scheme 3). In addition, the visual and fluorescence color changes owing to the Al^{3+} ions were not perturbed by the presence of an excess of biologically relevant alkali and alkaline earth metal ions (Na^+, K^+, Ca^{2+}, Mg^{2+}), transition metal ions

(Cr^{3+}, Mn^{2+}, Fe^{3+}, Co^{2+}, Ni^{2+}, Cu^{2+}, Zn^{2+}, Cd^{2+}), or other heavy metal ions (Hg^{2+}, Pb^{2+}), and these ions did not offer this type of visual and fluorescence color change through ring opening. Therefore, the organic moiety (**L**) has an excellent selectivity and specificity towards Al^{3+} ions over the other cations (Figures S11–S12).

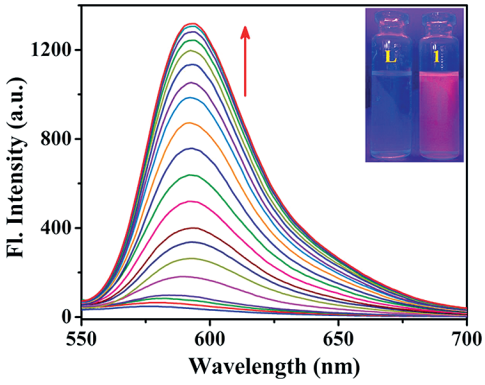

Figure 3. Emission spectra of **L** (10 μM) in HEPES buffer (1 mM, EtOH/water 1:9 v/v, pH 7.4) at 25 °C upon the incremental addition of Al^{3+} ions (0–20 μM); λ_{ex} = 525 nm. Inset: naked-eye fluorescence color change from **L** to **L**′–Al (**1**).

This selectivity for Al^{3+} ions over all other ions is due to selective chelate formation with **L** to afford an **L**′–Al complex (Scheme 3), which was found to have 1:1 stoichiometry through a Job plot of the fluorescence titration data (Figure S13). The probable formulation of the **L**′–Al complex was also verified by the isolation of the **L**′–Al complex in the solid state and its characterization by physicochemical and spectroscopic methods (Figures S5–S8). The selectivity of **L** towards Al^{3+} ions can also be ascribed to the strong binding constant (K) of 1.7×10^5 M^{-1}, as determined by the Benesi–Hilderbrand method (Figure S14).[13] To validate the sensitivity and affinity of **L** towards Al^{3+} ions, the detection limit was also calculated from the slope of the calibration curve (S) in the lower region (Figure S15) and the standard deviation of seven replicate measurements of the zero level (σ_{zero}) through the equation: detection limit = $3\sigma/S$, and it was found to be 17.3 nM.[14]

To establish the formation of the **L**′–Al species, a ^1H NMR titration of **L** in [D_6]dimethyl sulfoxide ([D_6]DMSO) was performed. The addition of Al^{3+} ions caused downfield shifts of some characteristic peaks (from δ = 3.699 to 3.684 ppm for the methoxy group) and a reduction of the singlet peak for the imine hydrogen atom (at δ = 9.00 ppm in **L**) with an upfield shift (δ = 8.98 ppm in **L**′–Al complex), but the peaks corresponding to the other hydrogen atoms of the phenyl and xanthene moieties did not show any significant changes (Figure S16). The formation of the **L**′–Al species through ring opening has also been ascertained from the ^{13}C NMR spectra of **L** in absence and presence of Al^{3+} ions, from which it was observed that the signal at δ = 66.225 ppm, attributable to the tertiary carbon atom (sp^3-hybridized) of the spirolactam ring in **L** (C-4), was absent in the spectrum of the **L**′–Al complex (Figures S3 and S7).[15]

A time-correlated single photon counting (TCSPC) experiment was also performed to measure the average fluorescence lifetimes (τ_{av}) of **L** and **L**′–Al at λ_{em} = 593 nm (Figure 4). From this study, it was observed that the average lifetime of the **L**′–Al species (2.54 ns) was greater than that of **L** (0.82 ns). From the equations $\tau^{-1} = k_r + k_{nr}$ and $k_r = \Phi_f/\tau$, in which k_r is the radiative rate constant and k_{nr} is the total nonradiative rate constant, the values of k_r and k_{nr} for both the organic moiety **L** and the **L**′–Al species were calculated and are tabulated in Table S3.[16] The values clearly indicate the enhancement of the fluorescence owing to the increase of the k_r/k_{nr} ratio from 0.03 to 1.4 through a chelation-enhanced fluorescence (CHEF) process.

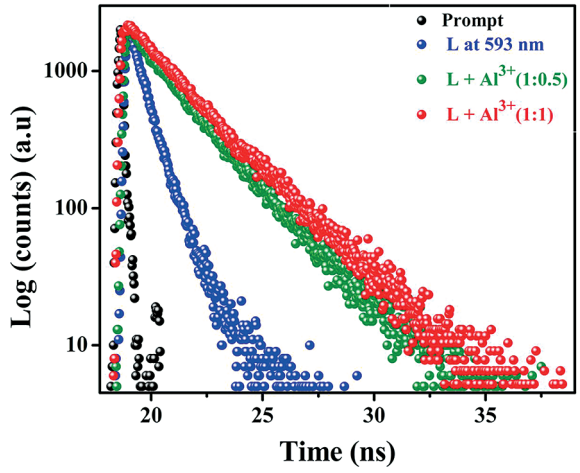

Figure 4. Time-resolved fluorescence decay of **L** (10 μM) and **L** in presence of added Al^{3+} ions in HEPES buffer (1 mM, pH 7.4) at 25 °C with a nano-LED of 550 nm as the light source; λ_{em} = 593 nm.

Interestingly, on treatment with F^- or OAc^- ions, the color of the **L**′–Al complex changed from pink to colorless and the fluorescence was quenched promptly (Figure 5).[17] On the basis of this observation, crystalline **L**′ in the *trans* conformation was obtained by treatment of an ethanolic solution of **L**′–Al with an ethanolic sodium fluoride solution in an equimolar ratio.

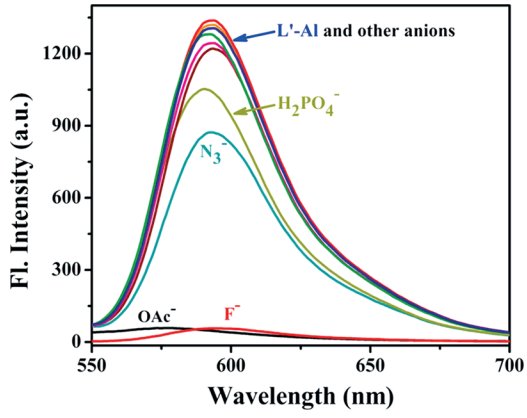

Figure 5. Anion selectivity of **L**′–Al in the presence of different anions in HEPES buffer (1 mM, EtOH/water 1:9 v/v, pH 7.4) at 25 °C.

The single crystals of **L′** (*trans* conformation) collected on slow evaporation of this reaction mixture were studied by single-crystal X-ray diffraction. The structural analysis of **L′** showed that the methoxy group of the phenyl ring is in a *trans* orientation with respect to the xanthene moiety (Figure 1, B). Compound **L′** crystallized in the monoclinic system in space group $P2_1/c$, whereas **L** (*cis* conformation) crystallized in the triclinic system in space group $P\bar{1}$. Although electron delocalization is present in the N1/N2/C8 fragment and there is a small amount of double-bond character in the N–N bond (the single N–N bond length is 1.47 Å, and an average value of 1.38 Å was measured here), the two molecules can be seen as different conformations that result from a rotation of ca. 180° about the N1–N2 bond. The C16–N1–N2–C8 torsion angles are 173.9° in **L′** and 13.7° in **L**. The molecules are closely comparable with a slight difference in the bending of the two phenyl groups of the rhodamine moiety, which form dihedral angles of 13.06 and 22.12° in **L′** and **L**, respectively. Under the same reaction conditions, this isolated **L′** gave a similar **L′**–Al species with Al^{3+} ions to that obtained from **L**. Furthermore, **L′** was also recovered from this isolated **L′**–Al complex upon treatment with F^-/OAc^- ions by following the above-mentioned procedure (Scheme 1).

Scheme 1. Detailed mechanistic pathway of metal-ion-induced conformational isomerization.

The UV/Vis spectrum of **L′** in HEPES buffer is identical to that of **L,** but the fluorescence intensity of **L′** is somewhat greater than that of **L** by a factor of ca. 2.5 (Figure S17). Upon the addition of 2.0 equiv. of Al^{3+} ions to the solution of **L**, an approximately 34-fold enhancement of the fluorescence intensity was observed with a increase in quantum yield from 0.03 to 0.59, and the same amount of added Al^{3+} ions to the solution of **L′** caused an increase of fluorescence of ca. 11 times, and the quantum yield changed from 0.2 to 0.59 (Table S4).

The energy values obtained from ground-state theoretical DFT calculations clearly indicate that both the highest occupied molecular orbital (HOMO) and the lowest unoccupied molecular orbital (LUMO) of **L′** (*trans* conformation) are more stabilized than those of **L** (*cis* conformation; Figure 6). In **L**, the electron density mainly resides on half of the xanthene moiety, and there is some electron density on the C=O moiety. However, in **L′**, the electron density is mainly on the full xanthene moiety with some on the C=O moiety. Energy optimization calculations revealed that the **L′**–Al complex is much more stable than the **L**–Al complex, as the energy gap between the HOMO and LUMO in the **L′**–Al complex (1.231 eV) is lower than that of the **L**–Al complex (2.369 eV). The UV/Vis spectra in water computed from time-dependent DFT (TDDFT) calculations show two important bands in the range λ = 300–550 nm. For **L**, the band at λ = 341.68 nm is dominated by the HOMO–2→LUMO excitation, the band at λ = 320.44 nm is dominated by the HOMO→LUMO+1 excitation, the band at λ = 287.78 nm is mainly due to HOMO→LUMO+3 transitions, and the band at λ = 274.21 nm is mainly due to HOMO–2→LUMO+1 transitions (Figure S18). The details of the vertical excitation energies, oscillator strengths, and salient transitions are shown in Table S7. For **L′**–Al, the band at λ = 528.54 nm is dominated by the HOMO–1→LUMO and HOMO–1→LUMO+1 transitions, the band at λ = 351.02 nm is mainly due to HOMO–5→LUMO, HOMO–2→LUMO, and HOMO–2→LUMO+1 transitions (Figure S19), as tabulated in Table S8. The detailed theoretical studies, including the TDDFT calculations (Table S5–S8), are in good agreement with the experimental observations.

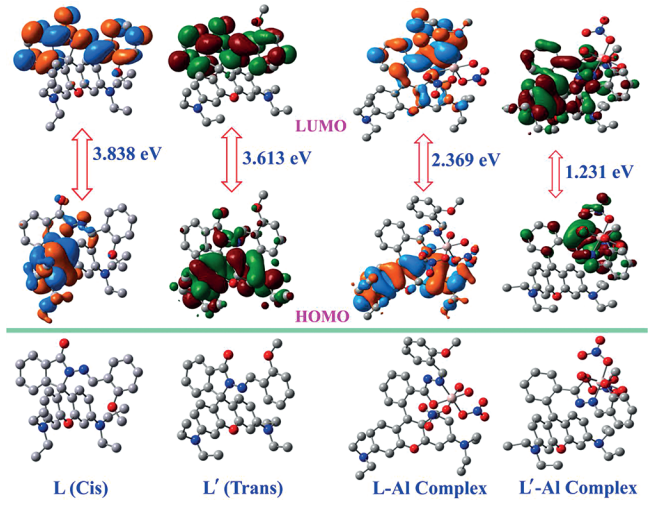

Figure 6. Molecular orbitals (MOs) of **L**, **L′**, and their corresponding Al complexes (H atoms are omitted for clarity).

Here, the coordination of Al^{3+} ions with the O atom of the C–O group of the rhodamine moiety and the imine N atom assists the *cis*-OMe group (with respect to the xanthene moiety) in **L** to overcome the steric hindrance between the *cis*-OMe group and the xanthene moiety and transform to its corresponding *trans* orientation through a rotation about the N–N bond. Thus, the **L′**–Al complex, formulated as $[Al(\mathbf{L'})(NO_3)_2(H_2O)_2][NO_3]$, is formed, and **L** (*cis* conformation) transforms into **L′** (*trans* conformation) in situ (Scheme 3). As a result of this type of complex formation, a chelation-enhanced fluorescence (CHEF) process was observed. Again, fluoride or acetate ions added to the solution of the **L′**–Al complex substituted the aqua molecules of the coordination sphere of the Al^{3+} ions to afford **L′** (*trans* conformation) from **L′**–Al (Scheme 3).

Additionally, the stability of the **L′**–Al species has also been examined by employing **L** in biological systems to acquire fluorescence images. Compound **L** was applied to human cervical cancer (HeLa) cells and breast cancer cells (MCF-7). A very faint intracellular fluorescence was captured after incubation with **L** (10 μM) for 30 min. However, the cells exhibited strong fluorescence when exogenous Al^{3+}

ions were applied into the cells (Figures 7, S20, and S22). In addition, an in vitro study showed no cytotoxic effects of **L** on the cells for up to 6 h, and the calculated IC_{50} value is greater than 50 μM (Figures S21 and S23).

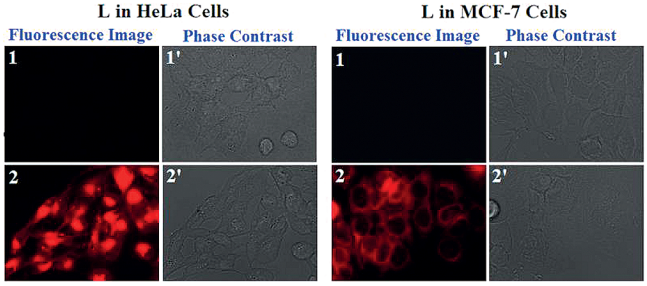

Figure 7. Fluorescence image of HeLa and MCF-7 cells after incubation with **L** (10 μM) for 30 min (1, 1′) followed by treatment with Al^{3+} ions (10 μM) at 37 °C (2, 2′).

Conclusions

This study represents the first manifestation of Al^{3+}-ion-induced conformational isomerization of a rhodamine derivative through a N–N bond rotation. The conformational change signals through a red fluorescence response and was studied through thorough structural characterization. Interestingly, this rhodamine derivative may be useful in the field of ion-controlled switching devices. Although there are a huge number of reports on rhodamine B derivatives as selective sensors for several ions through chelation-enhanced fluorescence (CHEF) or Förster resonance energy transfer (FRET) processes, it is notable that none of the resulting complexes or ensembles have been structurally established. As a result, it is not known whether the fluorescence changes occurred along with this type of structural change in the probes or not.[11c] Thus, this work will help us to explain this type of work in a proper way.

Experimental Section

Probe L: The probe **L** was synthesized by a two-step reaction (Scheme 2).

First, the rhodamine B hydrazide **1** was prepared by a literature method.[18] In brief, 85% hydrazine hydrate (4 mL) was added to a solution of rhodamine B (1 g, 2.09 mmol) in ethanol (40 mL). The solution was heated to reflux for 6 h. Then, the reaction mixture was evaporated under reduced pressure to give an orange oil, which was then recrystallized from methanol/water to afford rhodamine B hydrazide as light orange crystals (77%).

2-Methoxybenzaldehyde (136 mg, 1.0 mmol) was dissolved in ethanol, and this solution was added to an ethanolic solution of rhodamine B hydrazide (456 mg, 1.0 mmol) with stirring. Then, the resulting solution was heated to reflux for 6 h. The solution was evaporated to a small volume and cooled. The white crystalline product was collected by filtration and then recrystallized from pure methanol. Single crystals were obtained from this solution, one of which was selected for the crystallographic study, yield 78%, m.p. (178 ± 2) °C. $C_{36}H_{38}N_4O_3$ (574.70): calcd. C 75.24, H 6.66, N 9.75; found C 75.49, H 6.54, N 9.93. IR: $\tilde{\nu}$ = 3433 [$\nu_{OH(H_2O)}$], 3076 (ν_{NH}), 2968 [$\nu_{C=C(aromatic)}$], 1726 ($\nu_{C=O}$), 1614 ($\nu_{CH=N}$) cm^{-1}. ^1H NMR (300 MHz, [D_6]DMSO): δ = 9.00 (s, 1 H, CH=N), 7.87 (d, 1 H), 7.58–7.55 (m, 2 H), 7.54–7.47 (d, 1 H), 7.30 (t, 1 H), 7.05 (d, 1 H), 6.95 (d, 1 H), 6.87 (t, 1 H), 6.28–6.41 (m, 3 H), 3.69 (s, 3 H, OMe), 3.27 (q, 8 H, $4CH_2$), 1.04 (t, 12 H, $4CH_3$) ppm. ^{13}C NMR ([D_6]DMSO): δ = 164.530, 158.675, 153.589, 152.242, 149.356, 143.968, 134.676, 132.559, 129.755, 129.618, 128.518, 125.576, 124.752, 123.845, 123.652, 121.563, 112.931, 108.945, 106.251, 98.141, 66.225, 56.575, 44.590, 13.305 ppm. HRMS (ESI, ethanol): calcd. for $C_{36}H_{39}N_4O_3$ $[M + H]^+$ 575.2944; found 575.3147.

L′–Al Complex {[Al(L′)$(NO_3)_2(H_2O)_2$][NO_3]}: To an ethanolic solution (10 mL) of **L** (0.1 mmol, 58 mg), a solution of aluminium nitrate (0.1 mmol, 38 mg) was added dropwise, and the mixture was stirred for 4 h. The solvent was reduced to a small volume with a rotary evaporator, and the solution was kept in a beaker to afford a crystalline blood red solid on slow evaporation (Scheme 3). The pure solid was collected by filtration, washed with methanol, and then dried in vacuo. $C_{36}H_{42}AlN_6O_{11}$ (761.73): calcd. C 56.76, H 5.56, N 11.03; found C 56.57, H 5.50, N 11.17. IR: $\tilde{\nu}$ = 3452 (ν_{NH}), 1614 ($\nu_{C=N}$), 1383 [$\nu_{N-O(NO_3,sym)}$] cm^{-1}. ^1H NMR (300 MHz, [D_6]DMSO): δ = 8.98 (s, 1 H, CH=N), 7.87 (d, 1 H), 7.88–7.56 (m, 2 H), 7.53–7.46 (d, 1 H), 7.29 (t, 1 H), 7.05 (d, 1 H), 6.94 (d, 1 H), 6.87 (t, 1 H), 6.29–6.42 (m, 3 H), 3.68 (s, 3 H, OMe), 3.27 (q, 8 H, $4CH_2$), 1.04 (t, 12 H, $4CH_3$) ppm. ^{13}C NMR ([D_6]DMSO): δ = 165.060, 158.722, 153.486, 152.292, 151.006, 149.445, 143.566, 134.024, 132.728, 129.8805, 129.237, 128.502, 125.747, 124.644, 124.001, 123.359, 121.797, 112.979, 109.121, 105.998, 98.374, 56.581, 44.732, 13.227 ppm. HRMS (ESI, methanol): calcd. for $[M]^+$ 761.2727; found 761.3310 (ca. 10% abundance).

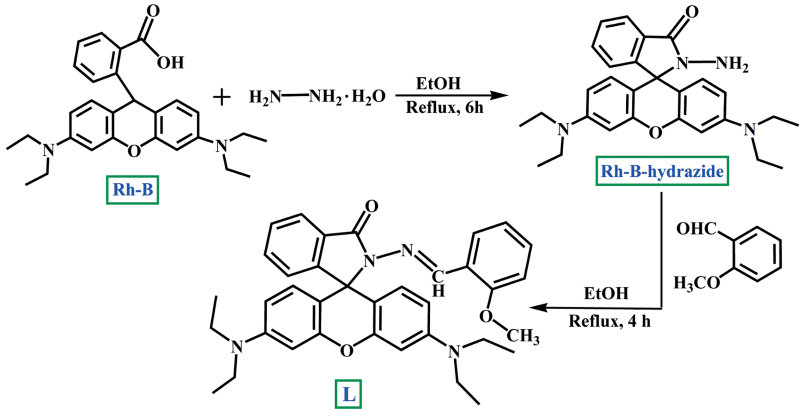

Scheme 2. Synthesis of the probe (**L**).

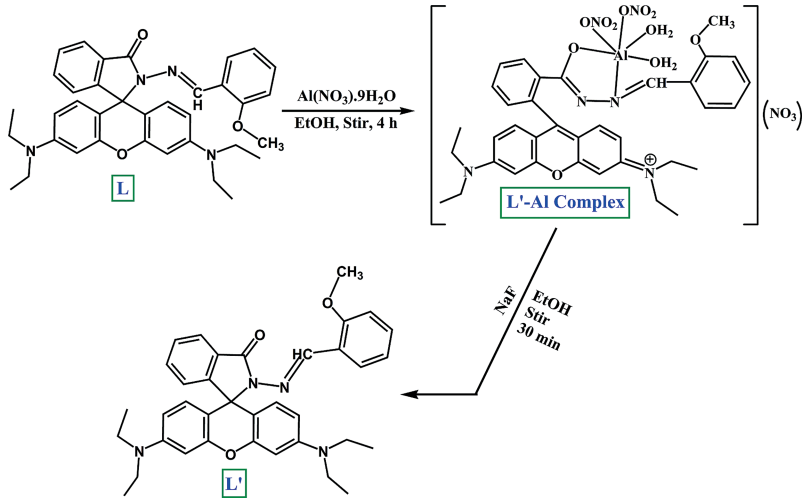

Scheme 3. Synthetic pathway for **L**′–Al and **L**′ from **L**.

Compound L′: To reclaim the probe from the **L**′–Al complex, we wanted to examine the quenching of fluorescence by adding different anions (CN^-, OAc^-, F^-, Cl^-, Br^-, I^-, N_3^-, $H_2PO_4^-$, NO_3^-, ClO_4^-, SO_4^{2-}, and $H_2AsO_4^-$) to ethanolic solutions of **L**′–Al complex. Interestingly, in this experiment, we noticed that the fluorescence of the **L**′–Al complex was dramatically quenched by the addition of only AcO^- or F^- anions, and no noticeable changes were observed with the other anions, as shown in Figure 5. Additionally, it is worth mentioning that this **L**′–Al complex can also be used as an AcO^-/F^- anion selective dual sensor.

On the basis of the above observation, an ethanolic solution of sodium fluoride (80 mg) was added to a solution of **L**′–Al (300 mg, 0.4 mmol) in ethanol (25 mL) with stirring. The mixture was stirred for 30 min at room temperature, and then the solution was kept aside. The crystalline **L**′ was obtained from this solution on slow evaporation within a few days; crystals suitable for single-crystal X-ray diffraction were also collected, yield 85%, m.p. (150 ± 2) °C. $C_{36}H_{38}N_4O_3$ (574.70): calcd. C 75.24, H 6.66, N 9.75; found C 75.52, H 6.58, N 9.96. IR: $\tilde{\nu}$ = 3460 [$\nu_{OH(H_2O)}$], 3076 (ν_{NH}), 2968 [$\nu_{C=C(aromatic)}$], 1762 ($\nu_{C=O}$), 1614 ($\nu_{CH=N}$) cm^{-1}. HRMS (ESI, ethanol): calcd. for $C_{36}H_{39}N_4O_3$ $[M + H]^+$ 575.2944; found 575.3021 (100%).

X-ray Crystallography: The X-ray data of suitable crystals of **L** and **L**′ were collected with a Bruker Apex-II CCD diffractometer with Mo-K_α radiation (λ = 0.71073). The data were corrected for Lorentz and polarization effects, and empirical absorption corrections were applied with SADABS from Bruker. The structures were solved by direct methods with SIR-92 and refined by full-matrix least-squares refinement methods based on F^2 with using SHELX-97.[19] All calculations were performed with the WinGX package.[20] Important crystallographic parameters are given in Table 1, and the corresponding bond lengths and angles are tabulated in Tables S1 and S2. CCDC-993884 (for **L**) and -1008295 (for **L**′) contain the supplementary crystallographic data for this paper. These data can be obtained free of charge from The Cambridge Crystallographic Data Centre via www.ccdc.cam.ac.uk/data_request/cif.

Theoretical Calculations: To clarify the understanding of the ground-state configurations of **L**, **L**′, and their corresponding complexes, DFT calculations were performed with the Gaussian-09 software over a Red Hat Linux IBM cluster. Molecular-level interactions have also been studied by density functional theory (DFT) with the B3LYP/6-31G (d,p) functional model and basis set.[21] Vertical electronic excitations based on B3LYP-optimized geometries were computed by the time-dependent density functional theory (TD-DFT)[22] formalism with water as the solvent, the conductor-like polarizable continuum model (CPCM)[23] was used to calculate the fractional contributions of various groups to each molecular orbital. The lowest 20 singlet states along the vertical excitation energies are computed here.

Preparation of Cell and in Vitro Cellular Imaging with L: Human cervical cancer cells (HeLa) and breast cancer cells (MCF-7) were purchased from the National Center for Cell Science (NCCS), Pune, India and used throughout the study. The cells were cultured in Dulbecco's modified Eagle's medium (DMEM, Gibco BRL) supplemented with 10% fetal bovine serum (FBS, Gibco BRL) and a 1% antibiotic mixture containing penicillin, streptomycin, and neomycin (PSN, Gibco BRL) at 37 °C in a humidified incubator with 5% CO_2. For the experimental study, the cells were grown to 80–90% confluence, harvested with 0.025% trypsin (Gibco BRL) and 0.52 mM ethylenediaminetetraacetic acid (EDTA; Gibco BRL) in phosphate-buffered saline (PBS, Sigma Diagnostics), plated at the desired cell concentration, and allowed to re-equilibrate for 24 h before any treatment. The cells were rinsed with PBS and incubated with DMEM containing **L** (10 μM, 1% DMSO) for 30 min at 37 °C. All experiments were conducted in DMEM containing 10% FBS and 1% PSN antibiotic. The imaging system was composed of a fluorescence microscope (ZEISS Axioskop 2 plus) with an objective lens [10×].

Cell Cytotoxicity Assay: To test the cytotoxicity of **L**, a 3-(4,5-dimethylthiazol-2-yl)-2,5-diphenyltetrazolium bromide (MTT) assay was performed by the procedure described previously.[24] After treatments of the probe (5, 10, 20, 50, and 100 μM), MTT solution (10 μL, 10 mg/mL PBS) was added to each well of a 96-well culture plate and incubated continuously at 37 °C for 6 h. All media were removed from the wells and replaced with acidic 2-propanol (100 μL). The intracellular formazan crystals (blue-violet) that formed were dissolved with 0.04 N acidic 2-propanol, and the absorbance of the solution was measured at 593 nm wavelength with a microplate reader. The values are means ± standard deviations (SDs) of three independent experiments. The cell cytotoxicity was calculated on the basis of a cell viability of 100%.

Supporting Information (see footnote on the first page of this article): Procedures, characterization data, and spectroscopic data.

Acknowledgments

The authors gratefully acknowledged the Council of Scientific and Industrial Research (CSIR), New Delhi for financial assistance. B. S. is thankful to the University Grants Commission (UGC), New Delhi for enabling him to do the work with a fellowship. The authors are also grateful to USIC, The University of Burdwan for the single-crystal X-ray diffractometer facility under the PURSE program and Prof. Ennio Zangrando, Dipartimento di Scienze Chimiche e Farmaceutiche, via Licio Giorgieri 1, 34127 Trieste, Italy for his generous help with structural elucidation.

[1] Y. Yang, Q. Zhao, W. Feng, F. Li, *Chem. Rev.* **2013**, *113*, 192.
[2] a) B. Sen, M. Mukherjee, S. Pal, K. Dhara, S. K. Mandal, A. R. Khuda-Bukhsh, P. Chattopadhyay, *RSC Adv.* **2014**, *4*, 14919; b) W. Shi, H. Ma, *Chem. Commun.* **2012**, *48*, 8732.
[3] a) S. Pal, B. Sen, M. Mukherjee, K. Dhara, S. K. Mandal, E. Zangrando, A. R. Khuda-Bukhsh, P. Chattopadhyay, *Analyst* **2014**, *139*, 1628; b) Y. Yang, S. K. Seidlits, M. M. Adams, V. M. Lynch, C. E. Schmidt, E. V. Anslyn, J. B. Shear, *J. Am. Chem. Soc.* **2010**, *132*, 13114.
[4] a) M. Takeuchi, M. Ikeda, A. Sugasaki, S. Shinkai, *Acc. Chem. Res.* **2001**, *34*, 865; b) R. Heck, F. Dumarcay, A. Marsura, *Chem. Eur. J.* **2002**, *8*, 2438; c) T. Nabeshima, Y. Yoshihira, T. Saiki, S. Akine, E. Horn, *J. Am. Chem. Soc.* **2003**, *125*, 28; d) J. Rebek Jr., *Acc. Chem. Res.* **1984**, *17*, 258.
[5] a) B. Armstrong, C. Tremblay, D. Baris, G. Thériault, *Am. J. Epidemiol.* **1994**, *139*, 250; b) D. Mozaffarian, A. Aro, W. C. Willett, *Eur. J. Clin. Nutr.* **2009**, *63*, S5; c) C. Chatgilialoglu, C. Ferreri, *Acc. Chem. Res.* **2005**, *38*, 441.
[6] W. J. Zhang, A. Berglund, J. Kao, J. P. Couty, M. Gershengorn, G. Marshall, *J. Am. Chem. Soc.* **2003**, *125*, 1221.
[7] W. You, H. Y. Zhu, W. Huang, B. Hu, Y. Fan, X. Z. You, *Dalton Trans.* **2010**, *39*, 7876.
[8] S. Owens, D. Smith, C. Lake, G. Grey, *Eur. J. Inorg. Chem.* **2008**, 4710.
[9] J. H. Cheng, Y. H. Zhang, X. F. Ma, X. G. Zhou, H. F. Xiang, *Chem. Commun.* **2013**, *49*, 11791.
[10] a) H. L. Ammon, S. K. Bhattacharjee, S. Shinkai, Y. Honda, *J. Am. Chem. Soc.* **1984**, *106*, 262; b) S. Shinkai, T. Nakaji, T. Ogawa, K. Shigematsu, O. Manabe, *J. Am. Chem. Soc.* **1981**, *103*, 111; c) K. Kimura, R. Mizutani, M. Yokoyama, R. Arakawa, G. Matsubayashi, M. Okamoto, H. Doe, *J. Am. Chem. Soc.* **1997**, *119*, 2062; d) V. W. W. Yam, V. C. Y. Lau, L. X. Wu, *J. Chem. Soc., Dalton Trans.* **1998**, 1461; e) V. W. W. Yam, Y. Yang, J. X. Zhang, B. W. K. Chu, N. Y. Zhu, *Organometallics* **2001**, *20*, 4911.
[11] a) J. Otsuki, K. Suwa, K. K. Sarker, C. Sinha, *J. Phys. Chem. A* **2007**, *111*, 1403; b) P. Gayen, C. Sinha, *Spectrochim. Acta Part A* **2012**, *98*, 116; c) A. K. Mandal, M. Suresh, P. Das, E. Suresh, M. Baidya, S. K. Ghosh, A. Das, *Org. Lett.* **2012**, *14*, 2980; d) D. Mallick, A. Nandi, K. K. Sarker, P. Datta, T. K. Mondal, C. Sinha, *Inorg. Chim. Acta* **2012**, *387*, 352; e) K. Li, Y. Xiang, X. Wang, J. Li, R. Hu, A. Tong, B. Z. Tang, *J. Am. Chem. Soc.* **2014**, *136*, 1643; f) Q. Sun, C. Zhang, L. Wang, Z. Li, A. Hu, Q. Tana, W. Xu, *Chem. Commun.* **2014**, *50*, 1728; g) J. Geng, T. Tao, H. Q. Chen, W. Huang, *Inorg. Chem. Commun.* **2014**, *42*, 23.
[12] a) V. W. W. Yam, X. X. Lu, C. C. Ko, *Angew. Chem. Int. Ed.* **2003**, *42*, 3385; *Angew. Chem.* **2003**, *115*, 3507; b) D. J. Hutchinson, M. P. James, L. R. Hanton, S. C. Moratti, *Inorg. Chem.* **2014**, *53*, 2122.
[13] H. A. Benesi, J. H. Hildebrand, *J. Am. Chem. Soc.* **1949**, *71*, 2703.
[14] A. Hakonen, *Anal. Chem.* **2009**, *81*, 4555.
[15] B. Sen, S. Pal, S. Lohar, M. Mukherjee, S. K. Mandal, A. R. Khuda-Bukhsh, P. Chattopadhyay, *RSC Adv.* **2014**, *4*, 21471.
[16] N. J. Turro, *Modern Molecular Photochemistry*, Benjamin/Cummings Publishing Co., Menlo Park, USA, **1978**.
[17] S. B. Maity, P. K. Bharadwaj, *Inorg. Chem.* **2013**, *52*, 1161.
[18] a) X. F. Yang, X. Q. Guo, Y. B. Zhao, *Talanta* **2002**, *57*, 883; b) V. Dujols, F. Ford, A. W. Czarnik, *J. Am. Chem. Soc.* **1997**, *119*, 7386.
[19] G. M. Sheldrick, *SHELXS97* and *SHELXL97*, University of Göttingen, Germany, **1997**.
[20] a) X. Zhou, P. Li, Z. Shi, X. Tang, C. Chen, W. Liu, *Inorg. Chem.* **2012**, *51*, 9226; b) A. Altomare, G. Cascarano, C. Giacovazzo, A. Guagliardi, *J. Appl. Crystallogr.* **1993**, *26*, 343; c) G. M. Sheldrick, *Acta Crystallogr., Sect. A* **2008**, *64*, 112; d) L. J. Farrugia, *J. Appl. Crystallogr.* **1999**, *32*, 837.
[21] a) M. Cossi, N. Rega, G. Scalmani, V. J. Barone, *Comput. Chem.* **2003**, *24*, 669; b) M. Cossi, V. Barone, *J. Chem. Phys.* **2001**, *115*, 4708; c) V. Barone, M. J. Cossi, *J. Phys. Chem. A* **1998**, *102*, 1995.
[22] M. E. Casida, C. Jamorski, K. C. Casida, D. R. Salahub, *J. Chem. Phys.* **1998**, *108*, 4439.
[23] N. M. O'Boyle, A. L. Tenderholt, K. M. Langner, *J. Comput. Chem.* **2008**, *29*, 839.
[24] a) J. Ratha, K. A. Majumdar, S. K. Mandal, R. Bera, C. Sarkar, B. Saha, C. Mandal, K. D. Saha, R. Bhadra, *Mol. Cell. Biochem.* **2006**, *290*, 113; b) S. Banerjee, P. Prasad, A. Hussain, I. Khan, P. Kondaiah, A. R. Chakravarty, *Chem. Commun.* **2012**, *48*, 7702.

Received: November 15, 2014
Published Online: February 9, 2015

